MMA Memo 197
Feed Leg Blockage and Ground Radiation Pickup for Cassegrain Antennas

Jingquan Cheng
email: jcheng@nrao.edu
and
Jeffrey G. Mangum
email: jmangum@nrao.edu
National Radio Astronomy Observatory
949 North Cherry Avenue
Tucson, AZ 85721

February 20, 1998

Abstract

This memo analyzes the changes in system temperature and scattered radiation termination location with feed leg attachment position and feed leg geometry. Calculation of the changes in system temperature with feed leg attachment radius shows that there is a relatively small penalty paid when the feed legs are attached inside the reflector surface. A ray tracing analysis of the termination locations for scattered radiation indicates that feed leg attachment to the edge of the antenna may not be the best configuration either from the total blockage point of view or from the spillover noise point of view.

1 Introduction

In this discussion, we will use the following definitions (see Figure 1):

f is the focal ratio for the primary reflector;

D is the primary reflector diameter;

l is the feed leg length;

w is the feed leg width;

h is the feed leg height;

I is the moment of inertia of the feed leg;

E is the Young's modulus of the feed leg;

B is the stiffness of the feed leg;

T_e is the edge taper in dB;

α is the edge taper factor;

β is the angle that the inner part of the feed leg makes with the axis of the telescope, which from Figure 1 is given by

$$\tan\beta = \frac{r_f - r'}{fD - \frac{r_f^2}{4fD}} \tag{1}$$

θ is the angle between the outgoing ray and the reflector aperture plane;

ϕ is the angle between the outgoing ray and the reflector axis;

r_0 is the telescope primary reflector radius;

r_f is the distance from the axis of the primary reflector to the point where the inner part of the feed leg attaches to the primary reflector;

r_{sub} is the subreflector hub diameter;

r' is the distance from the primary focus to the inner part of the feed leg;

r_t is the tapered reflector radius given by

$$r_t = \frac{r_0}{\sqrt{\alpha}} \tag{2}$$

R_f is the ratio between r_f and r_0;

R_ρ is the ratio between the angle formed by a ray reflected from the prime focus to the maximum prime focus reflected angle;

n_{leg} is the number of feed legs.

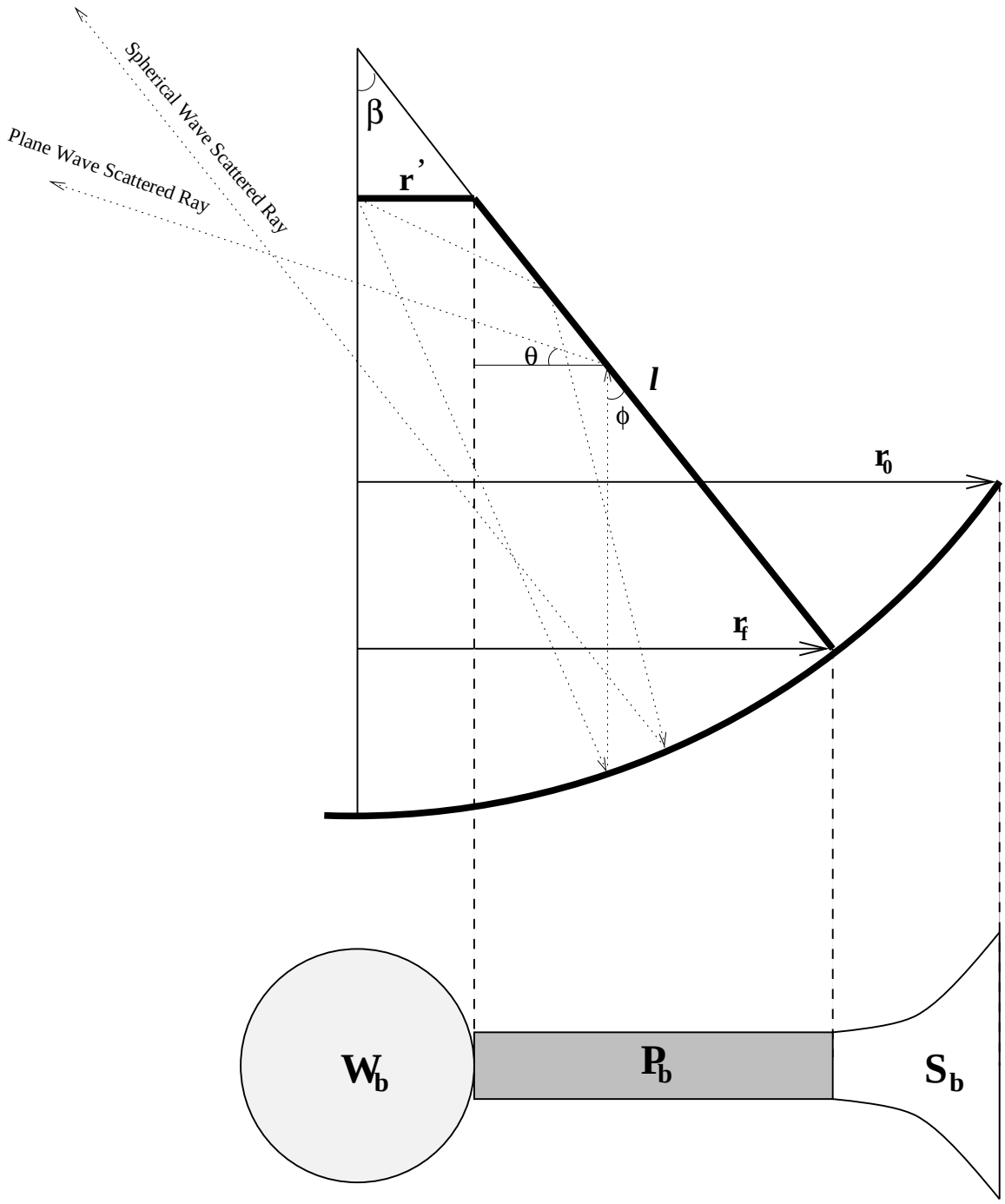

Figure 1: Geometrical definitions used in this memo. The lower part of the figure shows a geometrical representation of the three terms which contribute to the aperture blockage.

2 Contributions to the Total Blockage

The signal blockage in a Cassegrain system has three terms: blockage of the plane wave due to the central subreflector hub, blockage of the plane wave due to the feed legs, and blockage of the primary surface reflected (spherical) wave due to the feed legs. The form for each of these blockage terms is dependent upon the aperture illumination pattern. We will consider two types of illumination: uniform (Maanders 1975) and tapered gaussian (Lamb 1986). A good general discussion of this problem can be found in Ruze (1968). The voltage distribution function for these types of illumination pattern are given by

$$\begin{aligned} E(r) &= 1.0 && \text{(uniform)} \\ &= \exp\left[-\alpha\left(\frac{r}{r_0}\right)^2\right] && \text{(tapered gaussian)} \end{aligned} \tag{3}$$

where

$$\alpha \equiv \frac{T_e}{20}\ln 10 \tag{4}$$

The blockage due to the subreflector hub is given by

$$\begin{aligned} W_b &= \pi r_{sub}^2 && \text{(uniform)} \\ &= \pi r_{sub}^2\left\{1-\exp\left[-\left(\frac{r_0}{r_t}\right)^2\right]\right\} && \text{(tapered gaussian)} \end{aligned} \tag{5}$$

The plane wave blockage due to the feed legs is given by

$$\begin{aligned} P_b &= n_{leg}\, w(r_f - r_{sub}) && \text{(uniform)} \\ &= \frac{n_{leg}\sqrt{\pi} w r_t}{2}\left[erf\left(\frac{r_f}{r_t}\right) - erf\left(\frac{r_{sub}}{r_t}\right)\right] && \text{(tapered gaussian)} \end{aligned} \tag{6}$$

The spherical wave blockage due to the feed legs is given by

$$S_b = \frac{n_{leg} w}{r'}\left\{\frac{r_0^2}{2} - \frac{r_f^2}{2} - fD\tan\beta(r_0 - r_f) + \frac{\tan\beta}{12fD}(r_0^3 - r_f^3)\right\} \quad \text{(uniform)}$$

$$
\begin{aligned}
= \quad & \frac{n_{leg} w}{2r'} \left[r_t^2 \left\{ \exp\left(-\frac{r_f^2}{r_t^2}\right) - \exp\left(-\frac{r_0^2}{r_t^2}\right) + \right.\right. \\
& \left.\left. \frac{\tan\beta}{4fD} \left[r_f \exp\left(-\frac{r_f^2}{r_t^2}\right) - r_0 \exp\left(-\frac{r_0^2}{r_t^2}\right) \right] \right\} + \\
& \sqrt{\pi} r_t \tan\beta \left(fD - \frac{r_t^2}{8fD} \right) \\
& \left[erf\left(\frac{r_f}{r_t}\right) - erf\left(\frac{r_0}{r_t}\right) \right] \Bigg] \qquad \text{(tapered gaussian)} \qquad (7)
\end{aligned}
$$

where the Error Function erf(x) is given by

$$
erf(x) = \frac{2}{\sqrt{\pi}} \int_0^x \exp(-t^2) dt \qquad (8)
$$

The length of a feed leg is given by (see Figure 1)

$$
l = \sqrt{\left(fD - \frac{r_f^2}{4fD} \right)^2 + \left(r_f - r' \right)^2} \qquad (9)
$$

In the antenna design, the feed leg stiffness is a very important consideration. The feed leg stiffness is limited by the feed leg width. For a typical rectangular shaped feed leg, the moment of inertia is

$$
I = \frac{h w^3}{12} \qquad (10)
$$

The feed leg stiffness under distributed load conditions is represented by

$$
B = \frac{EI}{l^3} \qquad (11)
$$

From the above formulae, for a given feed leg stiffness the feed leg width can be reduced in proportion to its change in length. In the following, we apply this relationship in the blockage calculation. However, two effects associated with the feed leg dimensions will not be considered in this memo. The first is that changes in the feed leg support position are coupled to the requirements for the reflector stiffness. For reflector edge feed leg support, the reflector stiffness will be an important factor in reducing the feed leg overall stiffness. The second consideration which we do not address is the fact that we do not take into account the influences of the resonant frequencies of the antenna on the feed leg geometry. For all antenna diameters considered in the memo, the feed legs are assumed to have the same dimensions.

Table 1: Assumed Values Used in Calculations

focal ratio (f)	0.38
subreflector diameter (d_{sub})	$0.475 \times \frac{D}{8.0}$ m
feed leg width (w)	$0.06 \times \frac{l_{8m}}{l}$ m
feed leg depth (h)	0.20 m
primary focus to feed leg distance (r′)	$0.5 \times \frac{D}{8.0}$ m
number of feed legs (n_{leg})	4
observing frequency (ν)	230.0 GHz
source elevation (el)	45.0°
atmospheric opacity (τ_0)	0.1
ambient temperature (T_{amb})	−5.0 C
double sideband receiver temperature ($T_{rx}(DSB)$)	$4\left(\frac{h\nu}{2k}\right)$
image termination temperature (T_{image})	4.2 K
forward scattering and spillover efficiency (η_{fss})	0.73
minimum blockage 8m blockage efficiency (η_{b8})	0.98
minimum blockage 8m rear scattering, spillover and ohmic loss efficiency (η_{l8})	0.97
fraction of total area blocked for minimum blockage 8m (F_{b8}, uniform illumination)	2.149 %
(F_{b8}, 11dB edge-tapered gaussian)	2.603 %

3 MMA Antenna Blockage and System Temperature

In the following we estimate the effects of blockage to the system temperature for an 8, 10, 12, and 15m diameter telescope with both uniform and tapered gaussian illumination. In Table 1 we list our assumed parameters used in these calculations.

Figures 2 and 3 show the area blocked, and the contributions from the central hub, plane wave, and spherical wave to that blockage, as a function of the feed leg attachment radius r_f for both uniform and 11dB edge-tapered gaussian illumination functions. From these figures one sees that the spherical wave blockage term dominates for $r_f \leq \frac{3}{4}r_0$ in the uniform illumination case and for $r_f \leq \frac{5}{8}r_0$ in the 11 dB edge tapered case. Beyond these radii the plane wave term dominates, primarily because of the thicker feed leg necessary. Comparison of Figures 2 and 3 also shows that an edge taper minimizes the contribution of the spherical wave blockage term.

Figure 4 shows the fraction of the total area blocked for D = 8, 10, 12,

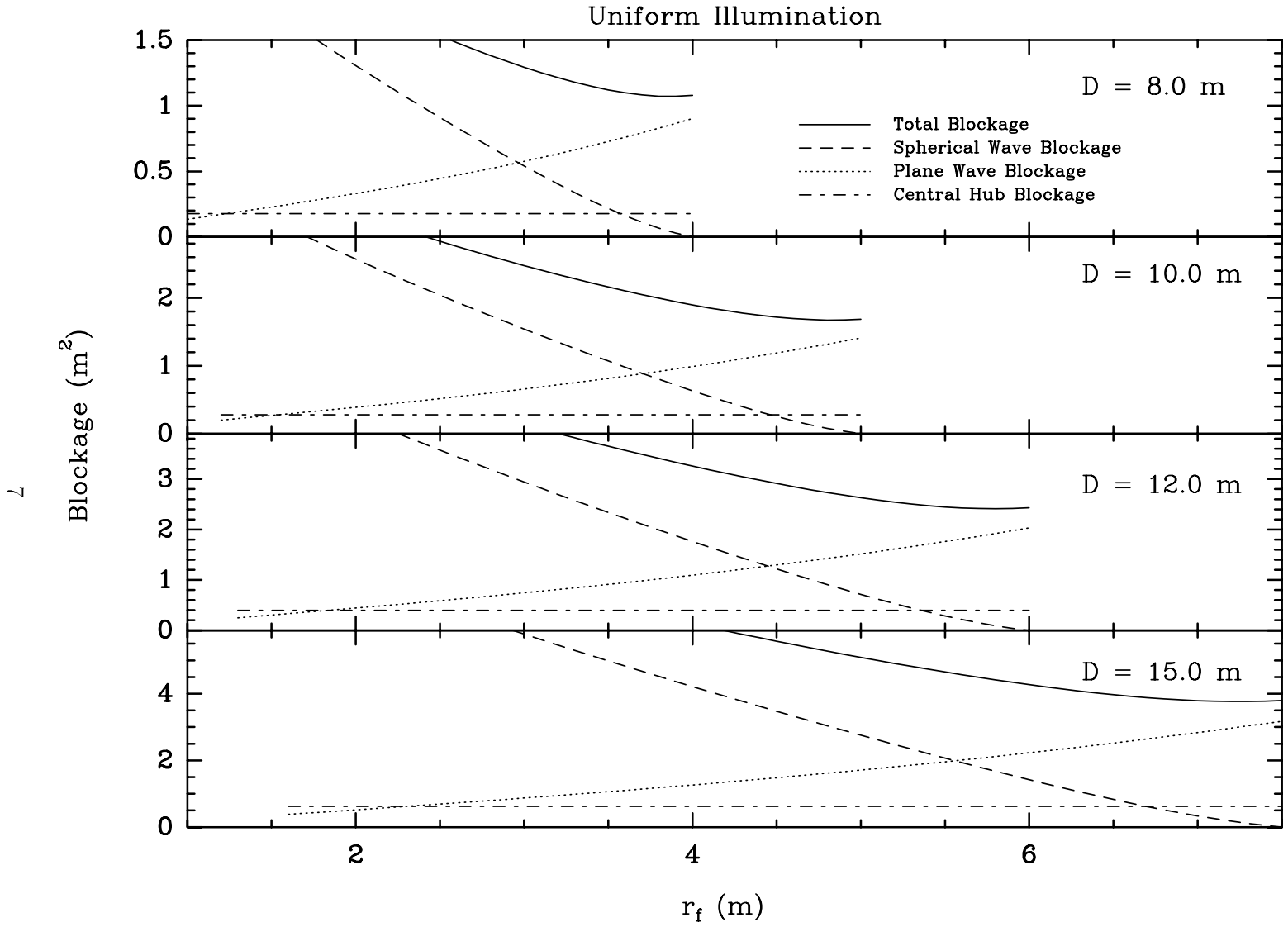

Figure 2: Total collecting area blocked as a function of the feed leg attachment radius r_f assuming a uniform illumination function and the assumed values given in Table 1.

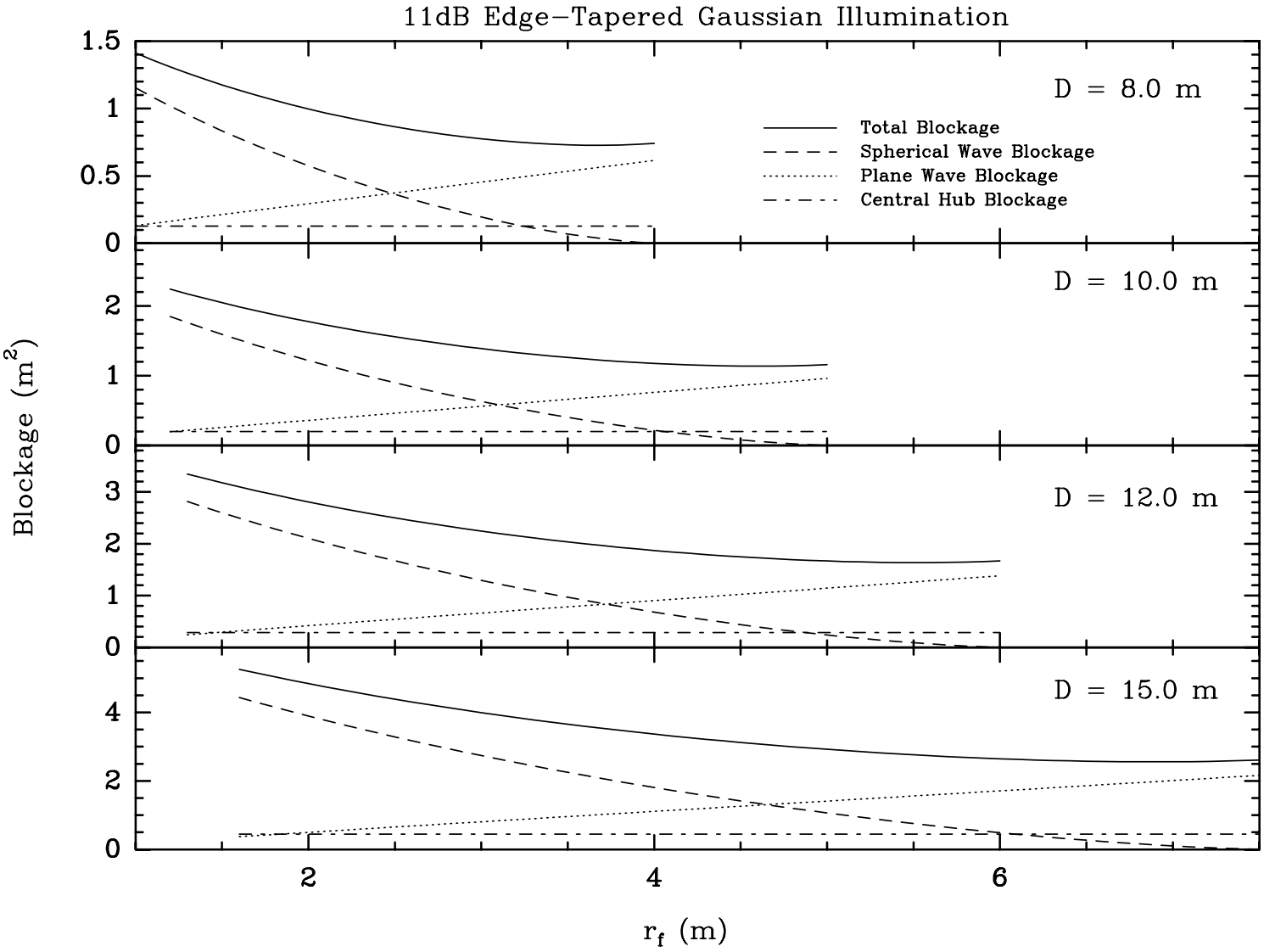

Figure 3: Total collecting area blocked as a function of the feed leg attachment radius r_f assuming an 11dB edge-tapered gaussian illumination function and the assumed values given in Table 1.

and 15m for both a uniform and an 11dB edge-tapered gaussian illumination function. Note that the total collecting area is given by

$$\begin{aligned} A_{collect} &= \pi r_0^2 \qquad \text{(uniform)} \\ &= \pi r_t^2 \left\{ 1 - \exp\left[-\left(\frac{r_0}{r_t} \right)^2 \right] \right\} \qquad \text{(tapered gaussian)} \end{aligned} \tag{12}$$

As in Figures 2 and 3, the effects of the edge taper are apparent. Note also that the slight increase in the blocked fraction as the feed leg encounters the edge of the reflector is due to the fact that we have assumed that the feed leg can be made narrower in proportion to its length.

To calculate the system temperature T^*_{sys} as a function of feed leg attachment radius, we use the assumptions listed in Table 1. The SSB system temperature of a single sideband system on the T^*_R scale (note that we drop the "*" in the following notation for simplicity) is given by the following equations (see MMA Memo 170 for details)

$$T^{ssb}_{sys}(SSB) = \frac{2T_{rx}(DSB) + T_A(sky) + T_{image}}{\eta_l \eta_{fss} \exp(-A\tau_0)} \tag{13}$$

The antenna temperature of the sky is given by the sum of noise contributions due to sky, antenna, and cosmic microwave background emission

$$\begin{aligned} T_A(sky) &= T^{cold}_{sky} + T^{hot}_{sky} + T_{ant} + T_{cmbr} \\ &= \eta_l \eta_{fss} T_M \Big[1 - \exp(-A\tau_0) \Big] + \eta_l \Big(1 - \eta_{fss} \Big) \Big[1 - \exp(-A\tau_0) \Big] T_M \\ &\quad + (1 - \eta_l) T_{spill} + \eta_l T_{bg} \exp(-A\tau_0) \\ &= \eta_l T_M \Big[1 - \exp(-A\tau_0) \Big] + (1 - \eta_l) T_{spill} + \eta_l T_{bg} \exp(-A\tau_0) \end{aligned} \tag{14}$$

where

T_M is the mean temperature of the atmosphere (given approximately by $\sim 0.95 T_{ambient}$. This quantity is frequency and weather dependent and can be given more accurately by atmospheric models.);

T_{spill} is the effective temperature of the rear spillover (also $\sim 0.95 T_{ambient}$);

T_{bg} is the background temperature (usually taken to be the cosmic background temperature of 2.7 K).

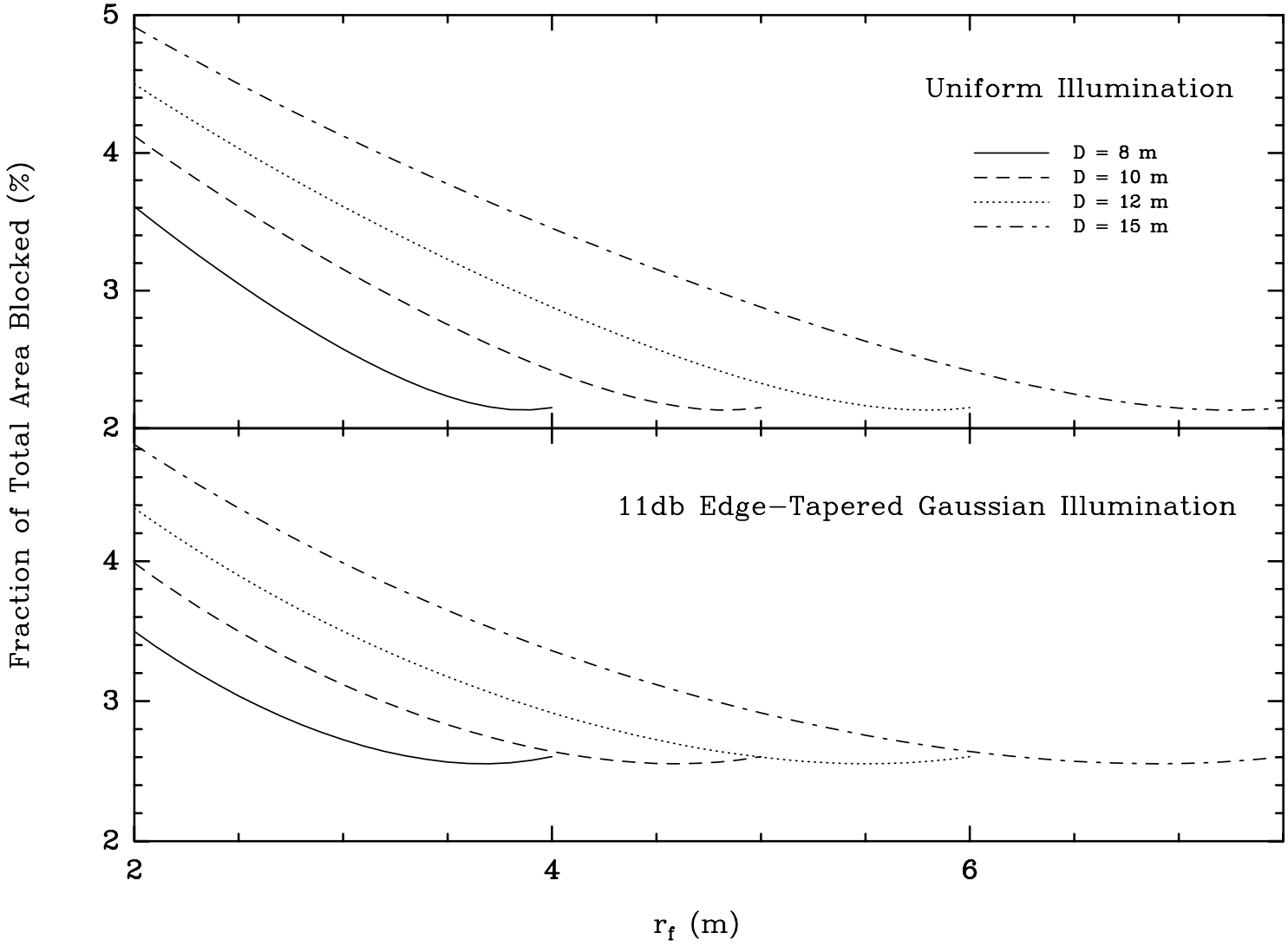

Figure 4: Fraction of total collecting area blocked for both a uniform and an 11dB tapered gaussian illumination function.

Since as the fractional area blocked increases as the aperture efficiency decreases, we can calculate the rear scattering and spillover efficiency as a function of feed leg attachment radius r_f using

$$\eta_l = \eta_{lmin}(1 - F_b)^2 \tag{15}$$

where F_b is the fraction of the total area blocked in the design under consideration and η_{lmin} is the rear scattering and spillover efficiency for the minimum blockage antenna for a given diameter. We further assume that the efficiencies for the minimum blockage design for each diameter are the same as that for the 8m diameter MMA design.

Figure 5 shows the system temperature T^*_{sys} as a function of the feed leg attachment radius r_f using the assumptions listed in Table 1. As expected, attaching the feed legs near the edge of the antenna reflector produces the lowest amount of ground pickup. The penalty for moving the feed legs inward, though, is quite small.

Two cases for the termination point of the scattered radiation are shown in Figure 5. The worst-case scenario ("Full Ground Termination" in Figure 5), where all of the scattered radiation terminates to warm ground, can easily be avoided. In the following, we describe how an appropriate choice of feed leg geometry can improve the scattering properties of a feed leg. An example of how this improvement translates to a reduced system temperature for a given attachment radius is shown in Figure 5 as the case where 50% of the scattered radiation terminates to warm ground and 50% terminates to cold sky.

4 Feed Leg Geometrical Considerations

In the following, we discuss the scattering of radiation from the traditional rectangular feed leg. Following this analysis, we consider the effects of shaping or baffling of feed legs to minimize ground radiation pickup.

4.1 Radiation Scattering From a Rectangular Feed Leg

In the previous section, the assumption is that all of the scattered radiation is terminated on the warm ground, which is the worst-case scenario. To understand the scattering of radiation due to feed legs at millimeter wavelengths, ray tracing is necessary. Referring to the feed leg geometry shown in Figure 1, if we trace rays from the center of the aperture, the rays will hit the secondary. After reflecting from the secondary, some rays blocked

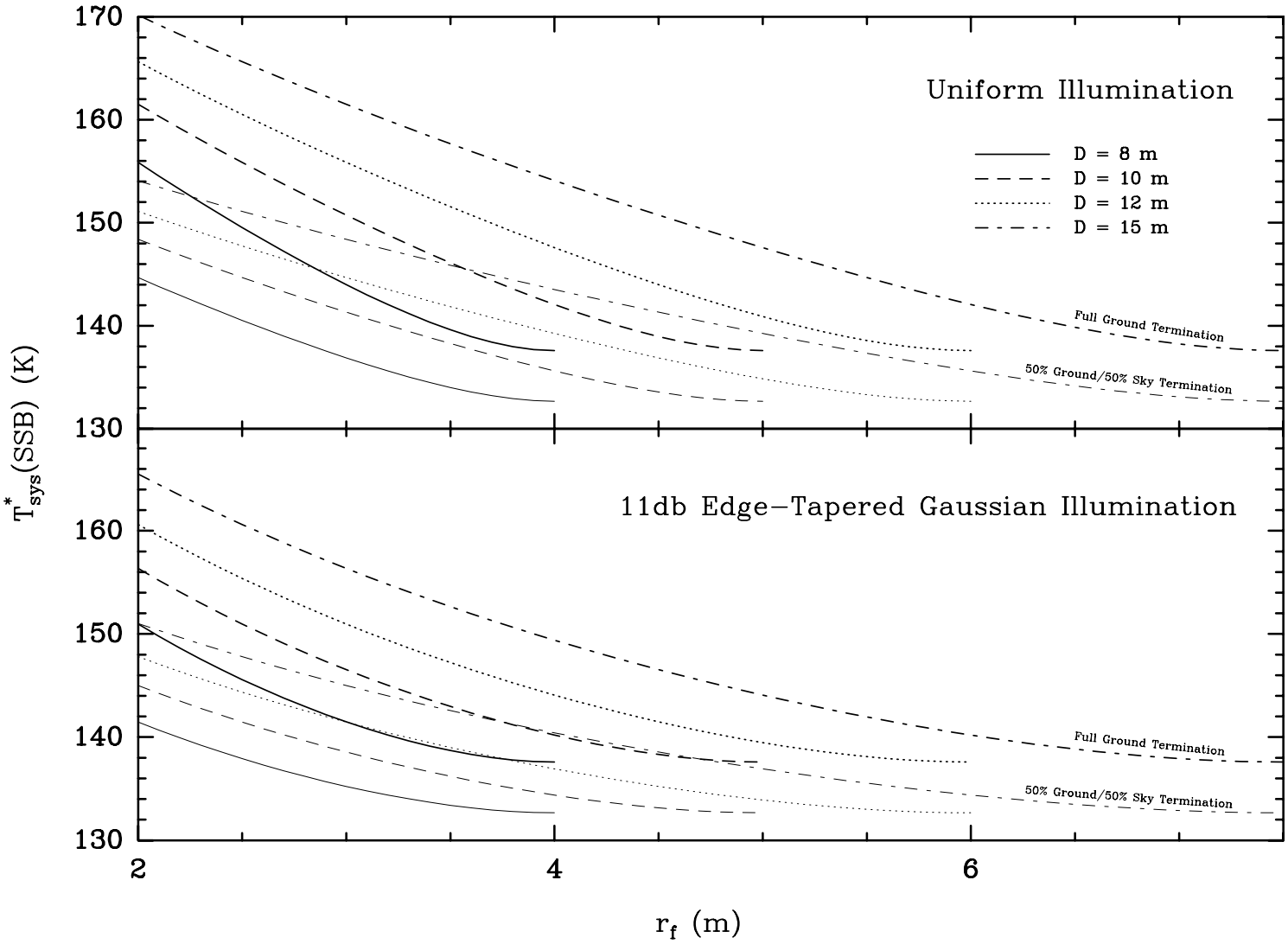

Figure 5: T_{sys} as a function of r_f using the assumptions listed in Table 1. Note also that we assume that the efficiency for the minimum blockage design for each diameter (η_{lmin}) is the same as that for the 8m diameter MMA design. Two cases of spillover radiation are shown. The darker lines for each diameter represent the case where all of the scattered radiation terminates on warm ground. The lighter lines for each diameter represent the case where 50% of the radiation terminates to cold sky and 50% to warm ground.

by the feed leg may reach the primary reflector first. These are called plane wave scattering rays. The other rays may reach the feed leg first. These are called spherical wave scattering rays.

The termination point for scattered radiation is a function of the feed leg geometry. Given the feed leg support radius r_f, the feed leg angle with the reflector axis will be:

$$\beta = \arctan\left(\frac{8f(r_f/r_0) - (r'/r_0)}{16f^2 - (r_f/r_0)}\right) \tag{16}$$

By taking $R_f = r_f/r_0$, and $R' = r'/r_0$ the β angle will be:

$$\beta = \arctan\left(\frac{8fR_f - R'}{16f^2 - R_f}\right) \tag{17}$$

Plane wave rays will have a direction parallel to the reflector axis after reflection from the primary reflector. The simple Snell law will give the direction of the reflected rays after the feed leg reflection. Taking ϕ as the angle of the reflected rays from the feed leg with the reflector axis (see Figure 1), ϕ will be:

$$\phi = 2\beta = 2\arctan\left(\frac{8fR_f - R'}{16f^2 - R_f}\right) \tag{18}$$

If we use the angle of the reflected ray above the aperture plane θ to represent the scattering direction, then $\theta = 90 - \phi$ (see Figure 1). Negative or smaller θ angles represent ground pickup at most observing directions. A higher θ angle represents no or little ground pickup at most observing directions.

Figure 6 shows the β and θ angles of the feed leg as a function of R_f. Note that $r' = \frac{r_0}{8}$ using the scaling law for r' given in Table 1. From Figure 6, the β angle increases from 0° to about 65° as the feed leg support radius increases, while the θ angle reduces greatly from 90° to a negative number. This figure considers only feed leg reflection and does not take into account what happens after reflection off of a feed leg. Interception of the scattered rays begins to occur for $\beta \simeq 45°$ (which corresponds to $\theta = 0°$). Full interception of the scattered radiation by the reflector occurs at the β angle of:

$$180 - 2\beta = \arctan\left(\frac{8f(1 + R')}{16f^2 - R_f}\right) \tag{19}$$

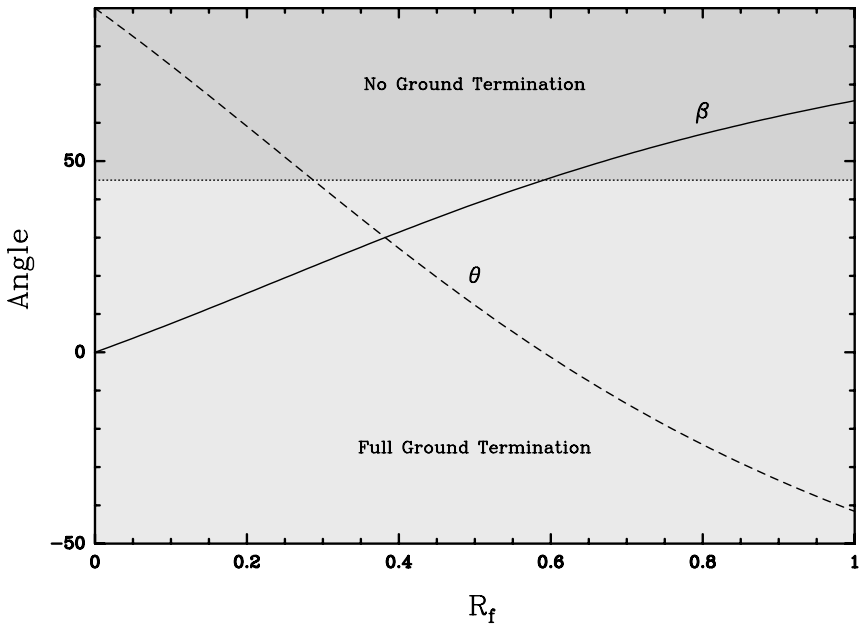

Figure 6: β and θ as a function of R_f. For $\theta < 0$ most scattered radiation terminates to warm ground, while for $\theta \gg 0$ most scattered radiation terminates to cold sky. The "No Ground Termination" and "Full Ground Termination" regions are drawn assuming an elevation angle of 45°.

Inserting Equation 1, the full-interception β angle occurs for $R_f \simeq 0.85$. After hitting the reflector again, the scattering rays will reflect above the aperture plane or hit the reflector a third time and end up terminated on cold sky. Spherical wave rays reflect off of the feed legs at very small incident angles, so will always fall on the reflector surface. Therefore the terminations of these rays should be high above the aperture plane.

For a thorough understanding of feed leg scattering, a ray tracing program has been written to analyze the problem. The program starts the ray tracing from the receiver horn. After the ray reaches the secondary mirror, the program follows the ray tracing to either the main reflector or the feed leg. Further ray tracing could be done either between these two reflecting surfaces or within the primary reflector itself. The ray reflected from the feed leg or primary mirror to the secondary mirror is not considered (the secondary mirror is small, so the effect is not significant). The ray tracing is done for different feed leg support radii R_f. After running this program, the resultant ray termination is shown in Figure 7.

Figure 7 shows the rectangular shaped feed leg scattering ray termination angle for different feed leg support radii. From this figure one can see that there are four groups of curves. The horizontal lines in θ shown as Region

A represent reflected radiation off of a feed leg. The continuation of these reflected rays is shown as Region B, which represents reflection from feed leg to antenna to sky. As the feed leg support radius R_f increases, the scattering ray angles above the aperture plane (θ) are reduced. When R_f is 0.8, θ is negative, so that all scattered radiation hits the ground directly, producing noise in the system as predicted.

Region B and C in Figure 7 represents plane wave scattered radiation intercepted by the reflector twice, or three times. Curves in Region B run from the top left down to the bottom right of the figure. The curve for $R_f = 1.0$ in Region C is a ray which reflects three times off of the reflector surface. The last region in Figure 7, Region D, represents the spherical wave scattering. As we predicted before, this scattered radiation always terminates to cold sky.

¿From this figure, one could find that the feed leg reflector edge support produces not a best solution for the antenna design from the ground noise pickup point of view. However moving the feed leg inwards may produce lower plane wave scattering. This will be discussed in the following section.

4.2 Radiation Scattering From a Shaped Feed Leg

In the past, Moreira *et al.*, Satoh *et al.*, and Lawrence *et al.* had extensive study on the issue of the ground spillover pickup and feed leg shaping or baffling. The ground spillover pickup by the feed leg could be greatly reduced either by shaping the feed leg, by adding a dielectric layer to the surface of the feed leg, or by adding baffles over the feed leg surfaces. These analyses are done by wave theory and existing examples are available only for relatively low frequency ranges (4-50 GHz).

One shaping technique is to attach a triangular roof on the inner side of the feed leg (Lamb 1998). By geometrical optics, if the half angle of the roof is α, then the reflected rays from these tapered feed legs will have:

$$\theta = 90 - 2\arcsin(\sin(\beta)\sin(\alpha)) \tag{20}$$

By adjusting the roof half angle, the scattering rays of the feed leg could all be terminated to cold sky independent of their incident angle on the feed leg. This is also the finding made by Lamb. Figure 8 shows Equation 20 as a function of α for representative values of β.

The roof angle of the feed leg will reflect the spherical rays from the secondary mirror outwards in radius. This makes the incident angle on the primary mirror reflection approach the incident angle of ray, which will cause the ray to hit the same location of the reflector if the feed leg is

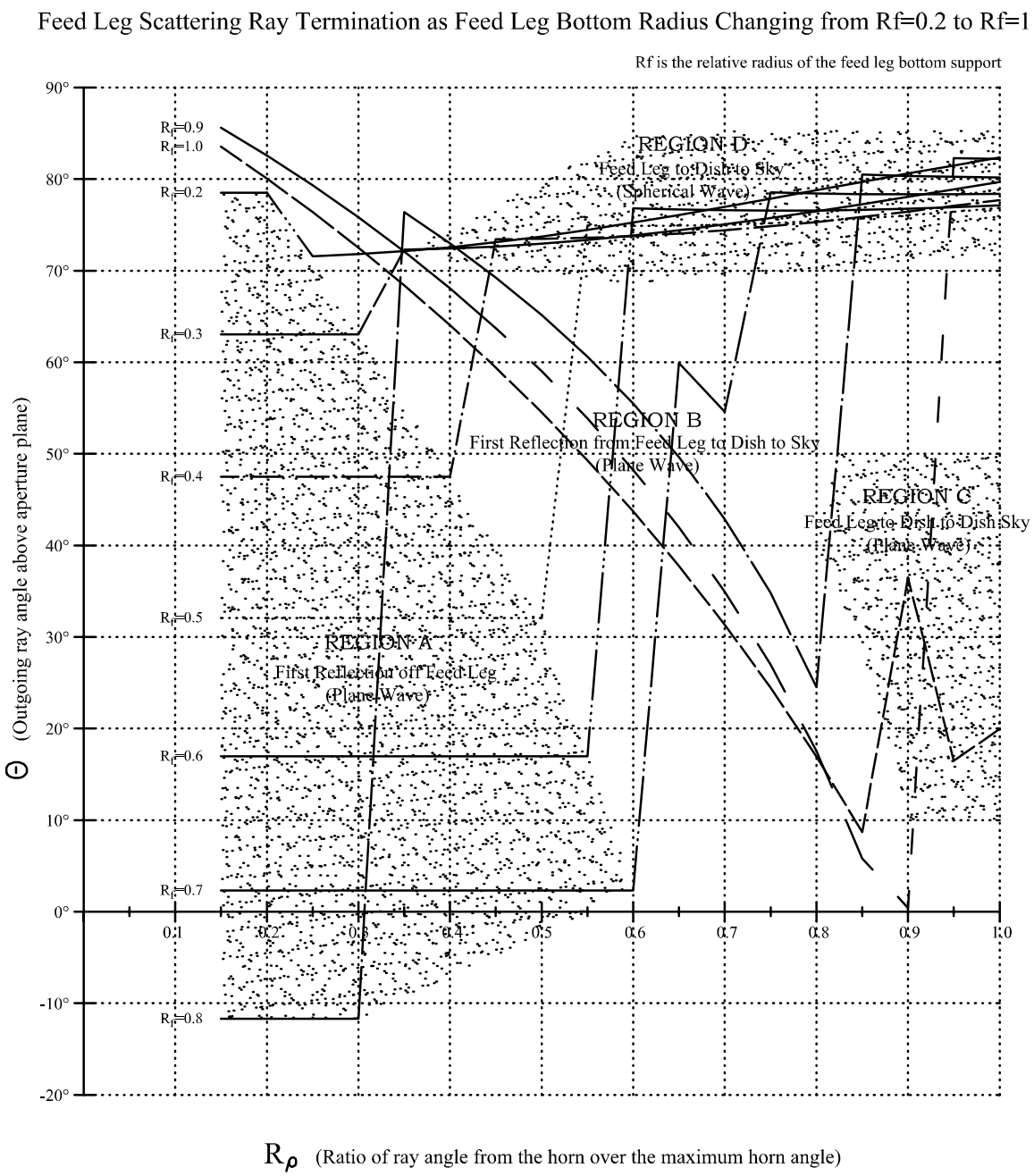

Figure 7: Ray tracing results. Four regions, representing four types of reflection from the feed legs and surface of the antenna, are indicated.

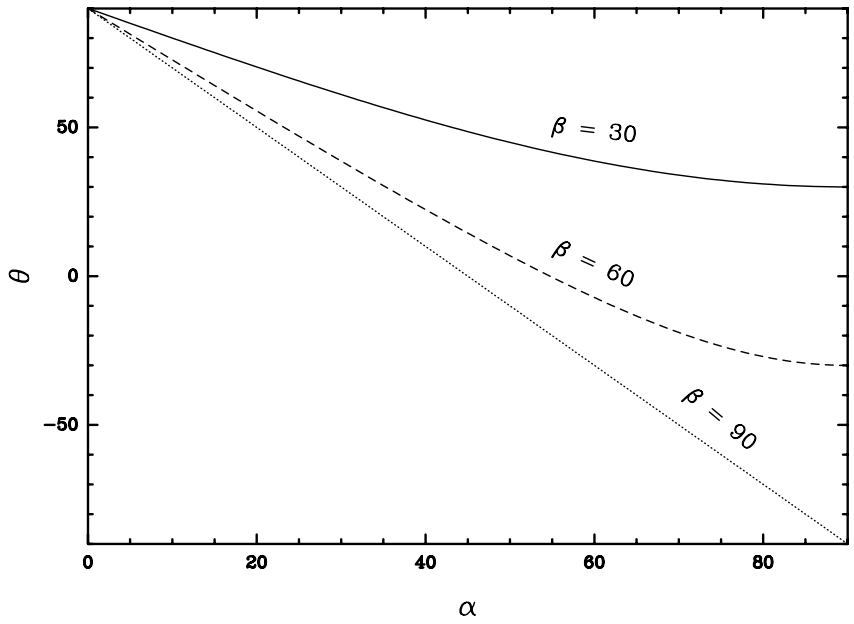

Figure 8: The scattered ray angle relative to the aperture plane θ as a function of the feed leg taper angle α for feed leg to reflector axis angles β of 30, 60, and 90°.

removed. Therefore, the spherical scattering rays will go even higher above the aperture plane as shown in Lamb (1998). Note also that the shaped feed leg will produce an angle change in the azimuth direction. This has little effect on the noise pickup.

5 Conclusions

1. Attaching the feed legs even as close as 2 meters from the axis of an 11dB edge-tapered antenna makes a contribution of between 8% (for D=8m) and 20% (for D = 15m) to the total system temperature at 230 GHz. The absolute contributions are 11 K and 28 K, respectively, for observations at an elevation of 45°, assuming that all of the scattered radiation terminates on warm ground (a worst-case scenario).

2. Feed leg attachment near the edge of the reflector represents a minimum blockage configuration. But, if a rectangular feed leg geometry is used, spillover noise pickup is greater than that for feed leg attachment inside the reflector. The scattered radiation pattern ranges from high elevation angle to very low elevation angle about the antenna aperture

plane.

3. To achieve lower noise due to feed leg radiation scattering, adding a triangular roof baffling on the inner side of the feed leg is an effective method. By using this method, the scattered radiation could be terminated to cold sky for any feed leg support radius.

4. The optimum feed leg support radius should be determined not by its scattering properties but by the structural requirements of the antenna.

6 References

Jewell, P. R. and Mangum, J. G., 1997, "System Temperatures, Single Versus Double Sideband Operation, and Optimum Receiver Performance", MMA Memo 170.

Lamb, J. W., 1998, Spillover Control on Secondary Mirror Support Struts, Internal Memo.

Lamb, J. W. & Olver, A. D., 1986, IEE Proceedings, 133, 43.

Lawrence, C. R., Herbig, T., & Readhead, A. C. S., 1994, Reduction of Ground Spillover in the Owens Valley 5.5m Telescope, IEEE Proc. 82, 763-767.

Maanders, E. J., 1975, "Enige Aspecten van Grondstation Antennes voor Satelliet Communicatie", Dissertation, State University of Gent, Belgium.

Moreira, F. J. S., Prata, A., & Thorburn, M. A., 1996, "Minumization of the Plane-Wave Scattering Contribution of Inverted-Y Strut Tripods to the Noise Temperature of Reflector Antennas", IEEE Trans AP-44, 492.

Ruze, J., 1968, Microwave Journal, 11, 76.

Satoh, T., Endo, S., Matsunaka, N., Betsudan, S., Katagi, T., & Ebisui, T., 1984, "Sidelobe Level Reduction by Improvement of Strut Shape", IEEE AP-32, 698.